Electronic Supplementary Material (ESI) for Dalton Transactions.

Supporting Information

Investigation of the magnetic anisotropy in a series of trigonal bipyramidal Mn(II) complexes

Moya A. Hay,[a] Arup Sarkar,[b] Katie E. R. Marriott,[a] Claire Wilson,[a] Gopalan Rajaraman,*[b]

and Mark Murrie*[a]

[a]WestCHEM, School of Chemistry, University of Glasgow, Glasgow, G12 8QQ (UK).

[b]Department of Chemistry, Institute of Technology Bombay, Powai, Mumbai, Maharashtra, 400 076 (India).

mark.murrie@glasgow.ac.uk, rajaraman@chem.iitb.ac.in

Contents

Table S1 Crystal Data and Structure Refinement Parameters

	1	**2**	**3**
Empirical formula	$C_{12}H_{25}Cl_3MnN_4$	$C_{14}H_{30}Cl_4MnN_4O_4$	$C_7H_{17}Cl_3MnN_2O$
Formula weight	386.65	515.16	306.51
Temperature/K	100(2)	100(2)	100(2)
Crystal system	trigonal	orthorhombic	monoclinic
Space group	R32	$Pca2_1$	$P2_1/m$
a/Å	10.628(3)	12.568(2)	7.8885(19)
b/Å	10.628(3)	12.844(2)	9.447(3)
c/Å	12.506(3)	13.236(2)	8.269(2)
α/°	90	90	90
β/°	90	90	96.572(6)
γ/°	120	90	90
Volume/Å^3	1223.4(6)	2136.6(7)	612.2(3)
Z	3	4	2
ρ_{calc}g/cm^3	1.574	1.601	1.663
μ/mm^{-1}	1.296	1.146	1.704
F(000)	603.0	1068.0	314.0
Crystal size/mm^3	0.5 × 0.2 × 0.1	0.5 × 0.1 × 0.1	0.6 × 0.2 × 0.1
Radiation	MoKα (λ = 0.71075)	MoKα (λ = 0.71075)	MoKα (λ = 0.71075)
2Θ range for data collection/°	5.496 to 51.486	3.172 to 51.676	4.958 to 51.366
Index ranges	$-12 \le h \le 11$, $-12 \le k \le 12$, $-15 \le l \le 15$	$-15 \le h \le 10$, $-15 \le k \le 11$, $-16 \le l \le 15$	$-9 \le h \le 7$, $-11 \le k \le 11$, $-9 \le l \le 10$
Reflections collected	4341	16680	11656
Independent reflections	529 [R_{int} = 0.0702, R_{sigma} = 0.0379]	4032 [R_{int} = 0.0886, R_{sigma} = 0.0878]	1236 [R_{int} = 0.1121, R_{sigma} = 0.0602]
Data/restraints/parameters	529/0/34	4032/1/247	1236/4/85
Goodness-of-fit on F^2	1.060	1.173	1.132
Final R indexes [I>=2σ (I)]	R_1 = 0.0221, wR_2 = 0.0516	R_1 = 0.0537, wR_2 = 0.1002	R_1 = 0.0445, wR_2 = 0.0981
Final R indexes [all data]	R_1 = 0.0225, wR_2 = 0.0518	R_1 = 0.0737, wR_2 = 0.1069	R_1 = 0.0636, wR_2 = 0.1059
Largest diff. peak/hole / e Å^{-3}	0.27/-0.28	0.78/-0.56	0.86/-0.49
Flack parameter	0.03(4)	0.03(5)	N/A

Table S2 Selected Bond Lengths for Complexes **1 - 3**

1		**2**		**3**	
Mn1··Cl1	2.4049(11) Å	Mn1··Cl2	2.390(2) Å	Mn1··Cl1	2.4273(12) Å
Mn1··Cl1′	2.4049(11) Å	Mn1··Cl3	2.382(2) Å	Mn1··Cl1′	2.4273(12) Å
Mn1··Cl1″	2.4049(11) Å	Mn1··Cl1	2.386(2) Å	Mn1··Cl2	2.3917(16) Å
Mn1··N1	2.363(3) Å	Mn1··N3	2.391(6) Å	Mn1··O1	2.202(4) Å
Mn1··N1′	2.363(3) Å	Mn1··N1	2.371(6) Å	Mn1··N1	2.342(5) Å

Table S3 Selected Bond Angles for Complexes **1 - 3**

1		**2**		**3**	
Cl1-Mn1-Cl1′	120.0	Cl2-Mn1-N3	93.06(16)	Cl1-Mn1-Cl1′	120.55(6)
Cl1′-Mn1-Cl″	120.0	Cl3-Mn1-Cl2	120.80(9)	Cl1-Mn1-Cl2	119.70(3)
Cl1-Mn1-Cl1″	120.0	Cl3-Mn1-Cl1	121.31(9)	Cl1′-Mn1-Cl2	119.70(3)
N1-Mn1-Cl1	90.0	Cl3-Mn1-N3	89.14(15)	O1-Mn1-Cl1	85.84(6)
N1-Mn1-Cl1′	90.0	Cl1-Mn1-Cl2	117.88(8)	O1-Mn1-Cl1′	85.84(6)
N1-Mn1-Cl1″	90.0	Cl1-Mn1-N3	88.80(15)	O1-Mn1-Cl2	95.90(12)
N1-Mn1-N1′	180.0	N1-Mn1-Cl2	91.17(16)	O1-Mn1-N1	168.65(16)
		N1-Mn1-Cl3	89.50(15)	N1-Mn1-Cl1	88.55(6)
		N1-Mn1-Cl1	88.41(16)	N1-Mn1-Cl1′	88.55(6)
		N1-Mn1-N3	175.7(2)	N1-Mn1-Cl2	95.44(12)
				Cl1′-Mn1-Cl1′	120.55(6)
				Cl1″-Mn1-Cl1′	119.70(3)

Figure S1 Crystal packing of **1** viewed along the *a*-axis (left) and *c*-axis (right). C, grey; Cl, green; Mn, lavender; N, blue. Hydrogen atoms omitted for clarity.

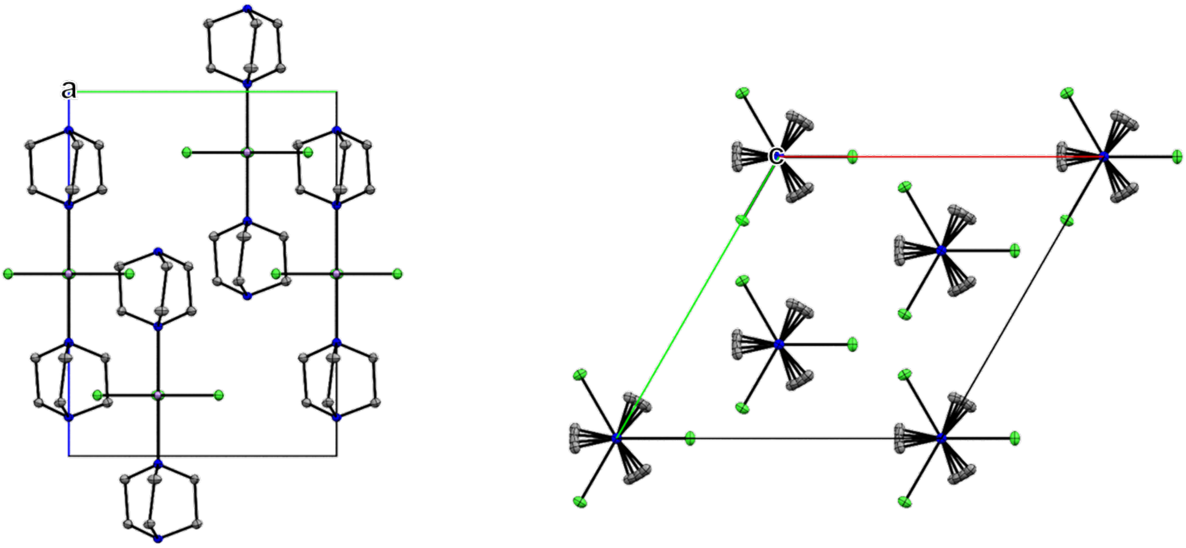

Figure S2 Crystal packing of **1** viewed along the *b*-axis with the N-H··N interactions highlighted in orange and the shortest Mn··Mn distances in blue. C, grey; Cl, green; Mn, lavender; N, blue. Hydrogen atoms omitted for clarity.

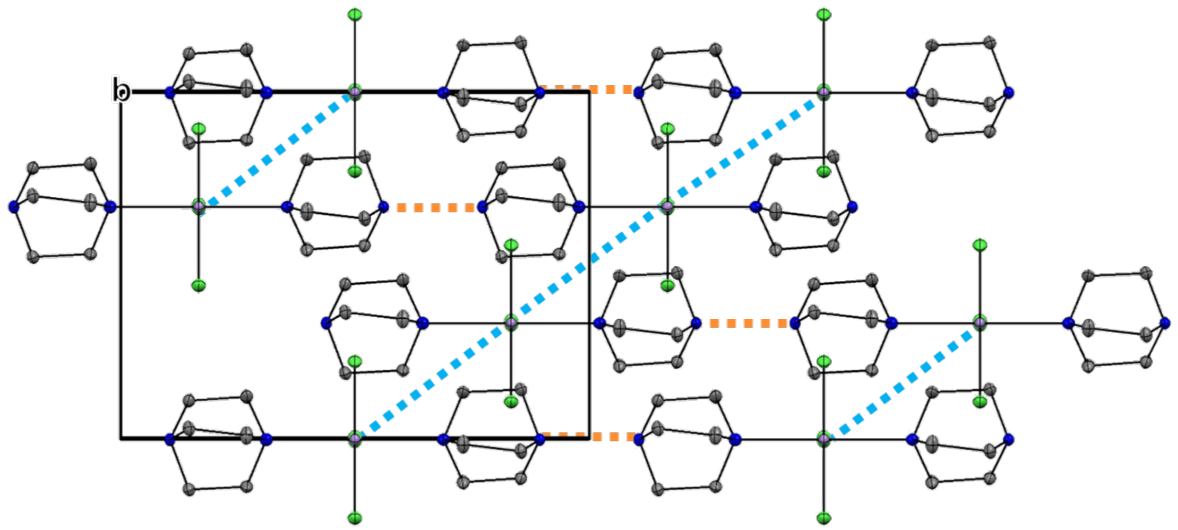

Figure S3 The asymmetric unit of **2** (left) with crystal packing shown on the right. Hydrogen atoms omitted for clarity.

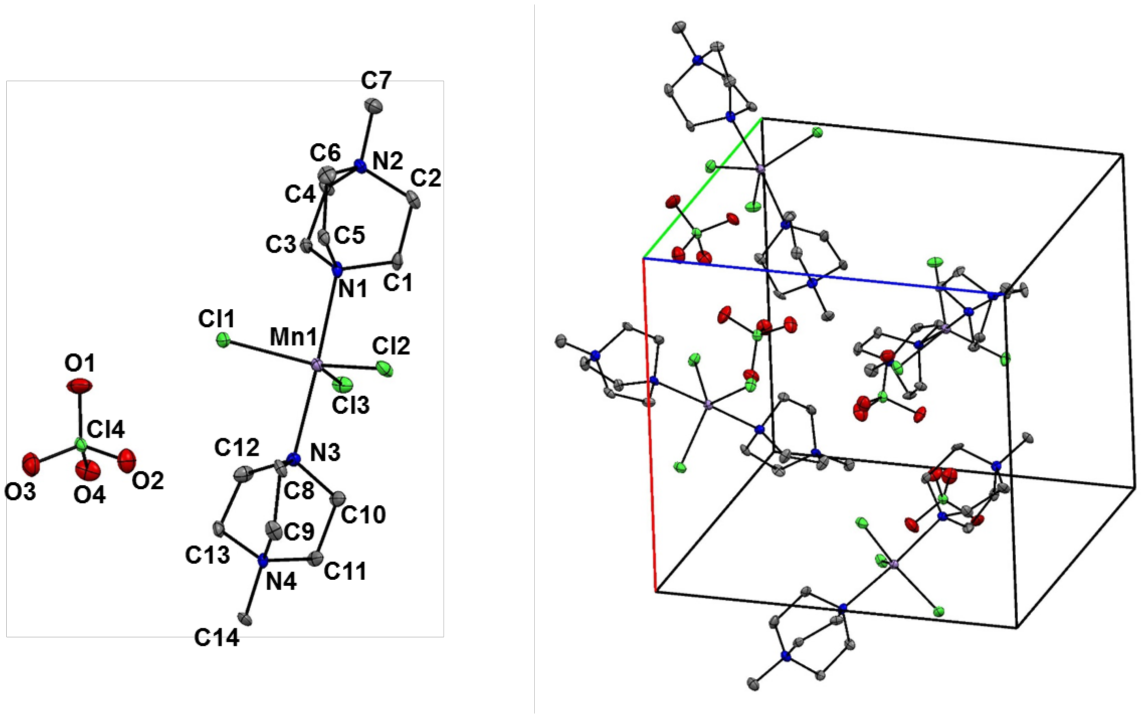

Figure S4 Structure of **3**, with the asymmetric unit shown on the left and the mirror plane associated with the $P2_1/m$ space group indicated in blue (right).

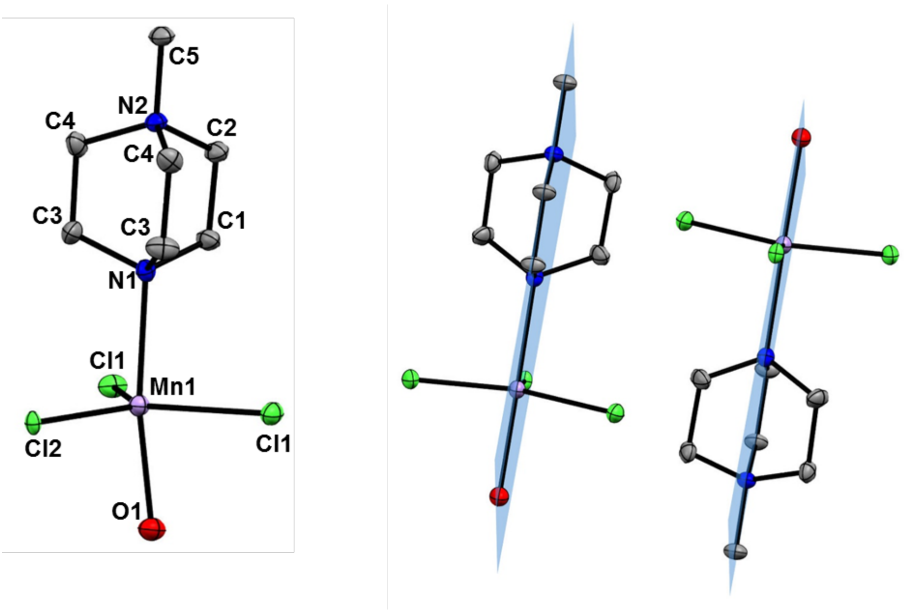

Table S4 Results from *SHAPE* studies[1,2] for complexes **1 - 3** with the lowest CShM value highlighted in purple signifying the closest geometry of the complexes, and the second closest highlighted in blue. The results show in each case the distortion is minimal, but increases on lowering of symmetry (**1** <**2** <**3**).

		CShM Values		
Shape	**Symmetry**	**1**	**2**	**3**
Pentagon	D_{5h}	37.118	36.010	35.996
Vacant Octahedron	C_{4v}	7.418	6.615	6.547
Trigonal Bipyramid	$\mathbf{D_{3h}}$	**0.007**	**0.061**	**0.393**
Spherical Square Pyramid	C_{4v}	5.381	4.478	3.783
Johnson Trigonal Bipyramid	D_{3h}	3.239	3.051	4.402

Figure S5 Depiction of the calculated powder X-ray diffraction (PXRD) of **1** based on single crystal XRD data collected at 100 K and the experimentally obtained powder X-ray diffraction collected at 290 K.

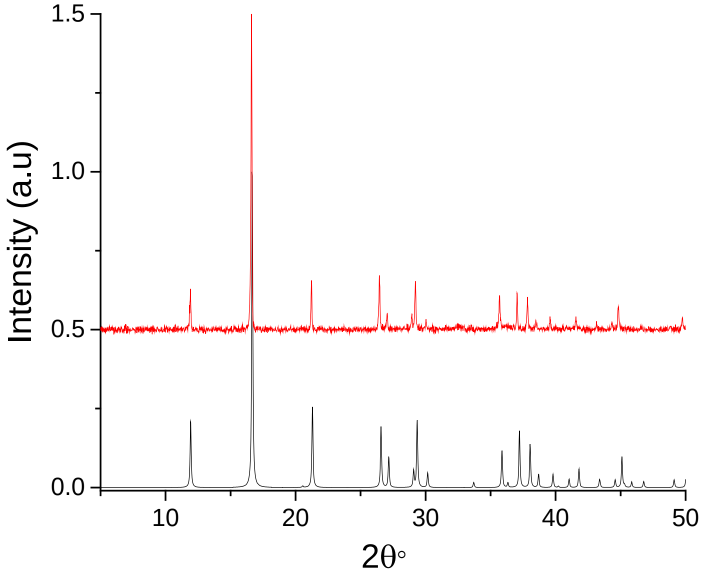

Figure S6 Depiction of the calculated powder X-ray diffraction (PXRD) of **2** based on single crystal XRD data collected at 100 K and the experimentally obtained powder X-ray diffraction collected at 290 K.

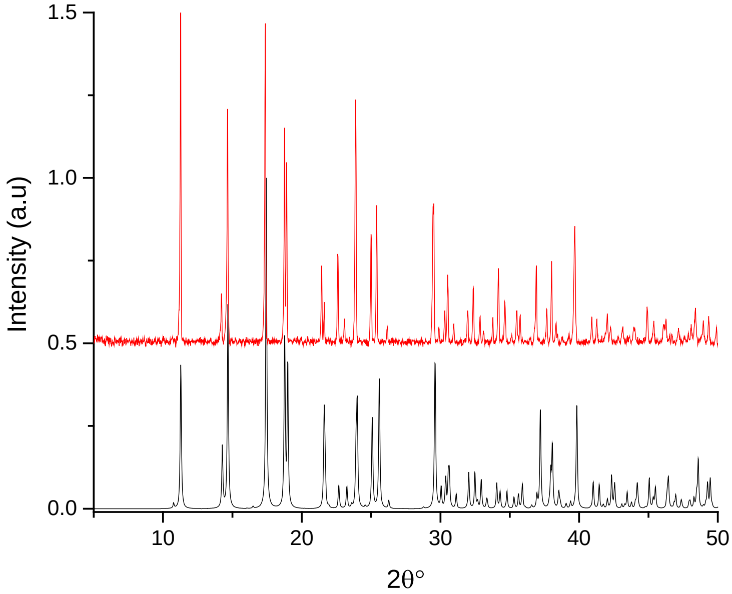

Figure S7 Depiction of the calculated powder X-ray diffraction (PXRD) of **3** based on single crystal XRD data collected at 100 K and the experimentally obtained powder X-ray diffraction collected at 290 K.

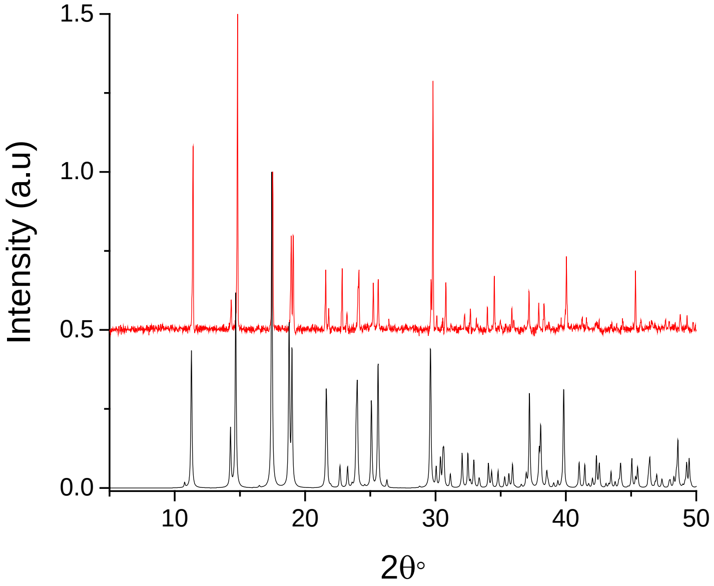

Figure S8 Magnetization versus field at 2, 4 and 6 K for complexes **1** (top), **2** (middle) and **3** (bottom). The solid lines for **1** and **2** correspond to the fit. Note, a fit of the *M* v *H* data corresponding to **3** was not possible. More details can be found in the *Magnetic Properties* section of the main article.

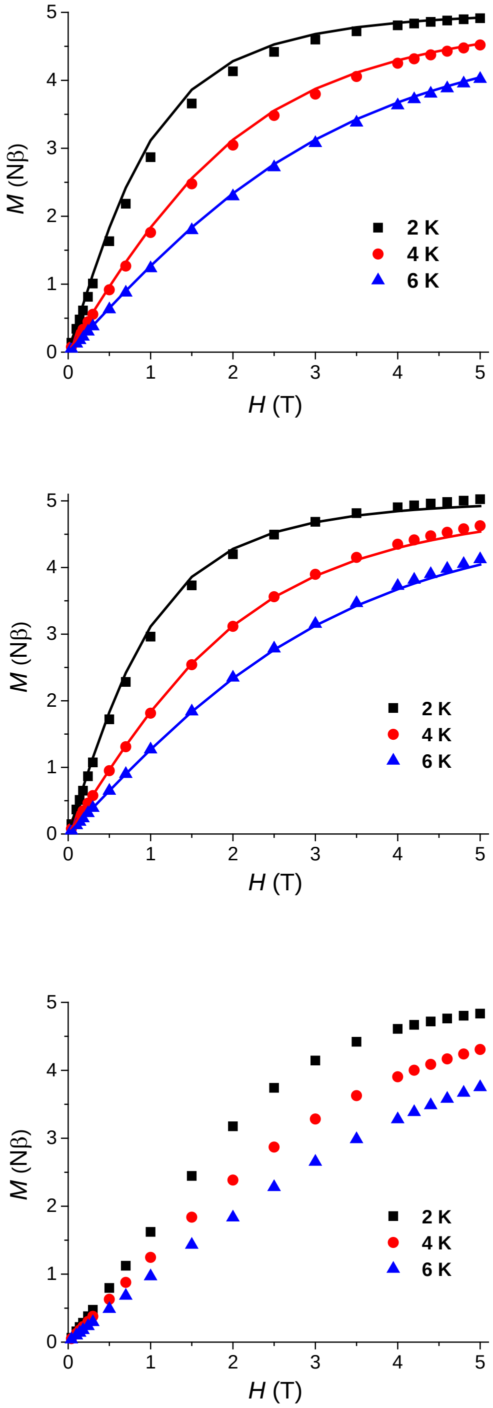

Additional Information Corresponding to the Fit of Magnetic Data

A parameter that accounted for the temperature independent paramagnetism (TIP) contribution towards the susceptibility was included in the Hamiltonian used to fit the data as shown in equation S1.[3] Additionally to the inclusion of the TIP parameter, a further parameter was included to account for a contribution originating from intermolecular interactions (equation S2). For each fit, a residual error was calculated using a sum of squares approach. In this case, the total value as opposed to an individual error for each set of data is calculated using equation S3.

$$\chi_{TIP} = \chi_{calc} + TIP \tag{S1}$$

$$\chi_{zJ} = \frac{\chi_{TIP}}{1 - \left(\frac{zJ}{N_A \mu_B^2}\right)} \tag{S2}$$

$$Residual = \left[\sum_{i=1}^{points} (M_{exp} - M_{calc})^2\right]\left[\sum_{i=1}^{points} (\chi_{exp} - \chi_{calc})^2\right] \tag{S3}$$

Figure S9 Alternating current (ac) susceptibility measurements for **1** at 0 Oe (left) and 2000 Oe (right) confirming that no out-of-phase response was detected.

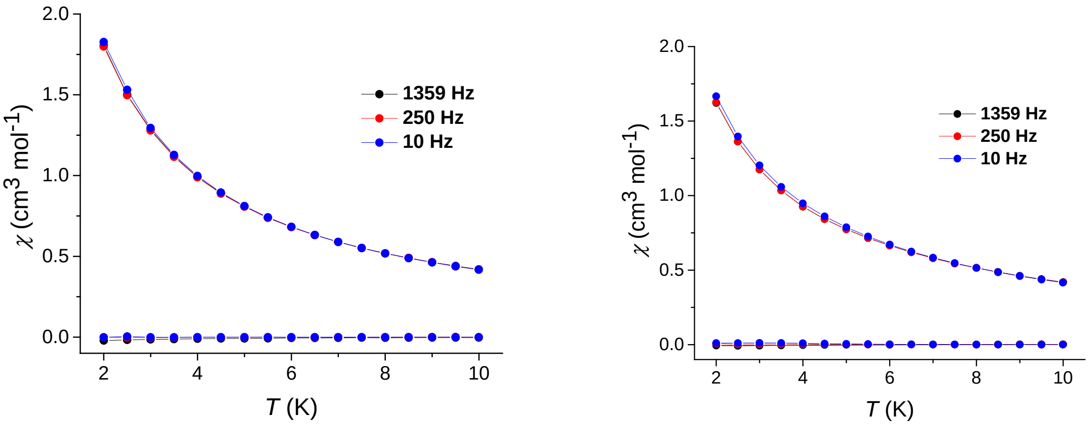

Figure S10 Alternating current (ac) susceptibility measurements for **2** at 0 Oe (left) and 2000 Oe (right) confirming that no out-of-phase response was detected.

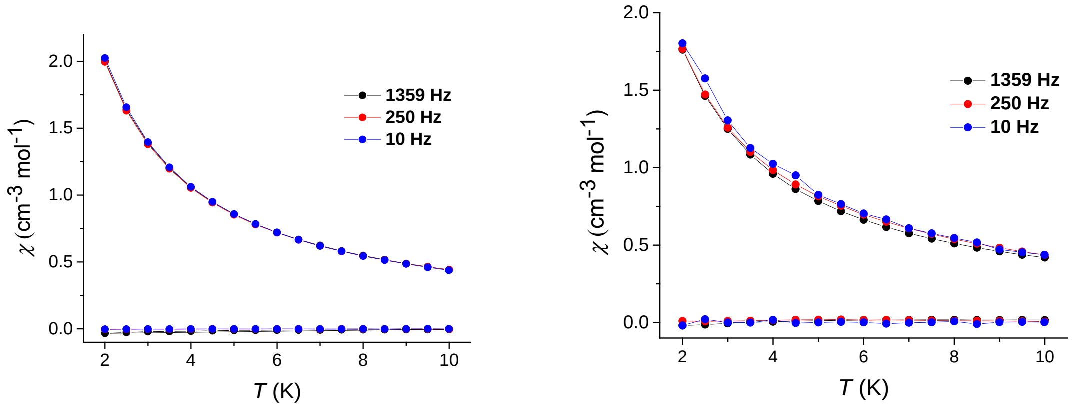

Figure S11 Alternating current (ac) susceptibility measurements for **3** at 0 Oe (left) and 2000 Oe (right) confirming that no out-of-phase response was detected.

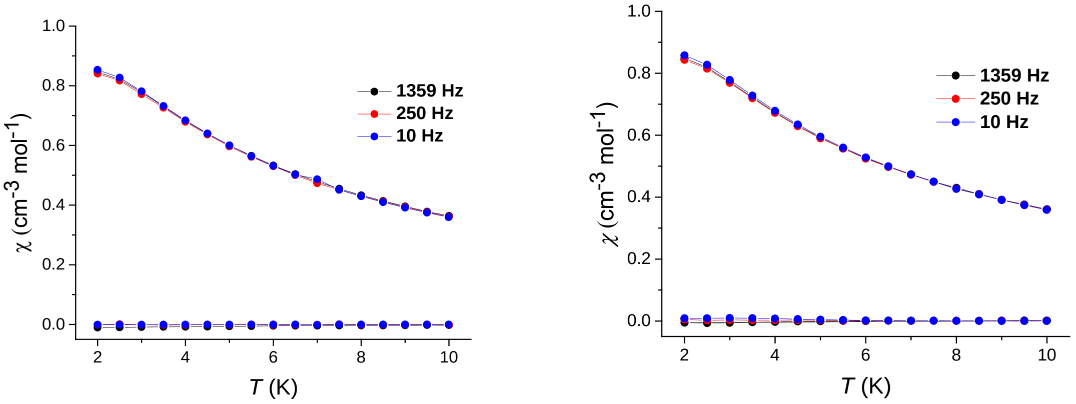

Computational Details

All the single point calculations on the three complexes have been performed in ORCA 4.0.0.[4,5] For the *ab initio* based approach to compute the Spin-Hamiltonian parameters, we performed complete active space self-consistent field (CASSCF) calculations. Prior to CASSCF, density functional theory (DFT) was performed to get the starting guess orbitals with ROKS level of theory and BP86 functional. The basis sets were chosen as- def2-TZVP on Mn and Cl, def2-TZVP(-f) on N, O and def2-SVP on C and H atoms. RIJCOSX approximation was incorporated during the DFT method to speed up the computation of the two-electron integrals with SARC/J taken as the auxiliary basis set on Mn, N, O and Cl and def2/J on rest of the atoms. In the configuration interaction (CI) step only the metal d-orbitals CAS(5,5) were taken into the active space since the molecules are prominently ionic in nature. During this step, 1 sextet, 24 quartet and 18 doublet roots were considered as it is sufficient for a high-spin Mn(II) complex. The basis sets were the same for this step except for the correlation effects, def2-TZVP/C for Mn, N, O and Cl and def2-SVP/C for C and H were chosen as auxiliary basis sets. To account for the dynamic correlation, N-electron valence perturbation theory 2nd order (NEVPT2) energy correction was also applied on the top of CASSCF calculations. In each step relativistic zeroth order regular approximation (ZORA) was incorporated both in the Hamiltonian as well in the basis sets. The final Spin-Hamiltonian parameters reported here are based on the effective Hamiltonian approach (EHA).[6] Furthermore, density functional calculations employing the CP method, as implemented in ORCA, have been utilised to compute the ZFS parameters for complexes **1-3**. Here we have estimated both the D_{SS} and D_{SOC} part employing the BP86/def2-TZVP setup (see Table S8).

Table S5 NEVPT2 transition energy and their individual contribution to the *D* values for complex **1** (up to 17 quartets and 13 doublets are shown).

Complex 1	**NEVPT2 energy (cm^{-1})**	**Contribution to D (cm^{-1})**	**Contribution to E (cm^{-1})**
^6S	000.0	0.000	0.000
^4G	22037.6	-0.315	-0.267
	22039.4	-0.315	0.267
	26515.6	0.000	0.000
	26649.0	0.000	0.000
	26950.0	0.000	0.000
	26950.6	0.000	0.000
	27241.5	0.000	0.000
	27242.1	0.000	0.000
	27394.9	0.000	0.000
^4P	29899.9	1.525	0.000
	31059.5	-0.026	0.022
	31062.4	-0.026	-0.022
^4D	32051.7	0.000	0.000
	32051.8	0.000	0.000
	32573.5	0.000	0.000
	34567.8	-0.476	0.41
	34571.5	-0.475	-0.41
^2I	33493.4	0.000	0.000
	33493.7	0.000	0.000
	35483.5	0.000	0.000
	35483.5	0.000	0.000
	36024.1	0.000	0.000
	36118.7	0.000	0.000
	36762.0	0.000	0.000
	36765.1	0.000	0.000
	37063.0	0.000	0.000
	37063.1	0.000	0.000
	39389.0	0.000	0.000
	39722.2	0.000	0.000
	39722.3	0.000	0.000

Table S6 NEVPT2 transition energy and their individual contribution to the *D* and *E* values for complex **2** (up to 17 quartets and 13 doublets are shown).

Complex 2	NEVPT2 transition energy (cm^{-1})	Contribution to *D* (cm^{-1})	Contribution to *E* (cm^{-1})
^6S	000.0	0.000	0.000
^4G	22141.1	-0.314	-0.291
	22286.5	-0.303	0.279
	26402.0	0.000	0.000
	26540.3	0.001	0.000
	26944.7	0.001	0.000
	27007.3	0.000	0.000
	27168.3	0.000	0.000
	27196.5	0.001	0.000
	27361.6	0.000	0.000
^4P	29835.1	1.508	0.000
	30844.8	-0.037	0.037
	31007.8	-0.046	-0.045
^4D	32115.8	0.001	0.000
	32158.7	0.007	-0.001
	32512.5	-0.004	0.001
	34307.4	-0.470	0.470
	34571.3	-0.455	-0.455
^2I	33521.9	0.000	0.000
	33652.3	0.000	0.000
	35666.6	0.000	0.000
	35669.0	0.000	0.000
	36102.2	0.000	0.000
	36206.8	0.000	0.000
	36749.1	0.000	0.000
	36959.9	0.000	0.000
	37155.7	0.000	0.000
	37233.4	0.000	0.000
	39327.6	0.000	0.000
	39696.1	0.000	0.000
	39700.0	0.000	0.000

Table S7 NEVPT2 transition energy and their individual contribution to the *D* and *E* values for complex **3** (up to 17 quartets and 13 doublets are shown).

Complex 3	**NEVPT2 transition energy (cm^{-1})**	**Contribution to D (cm^{-1})**	**Contribution to E (cm^{-1})**
^6S	000.0	0.000	0.000
^4G	22060.4 22714.8 26726.4 26826.6 27037.1 27094.5 27339.8 27353.8 27558.8	-0.32 -0.296 0.000 0.003 0.003 0.000 0.001 0.000 0.000	-0.32 0.296 0.000 0.000 0.000 0.000 0.000 0.000 0.000
^4P	30036.2 31361.9 31412.9	1.512 -0.009 -0.027	0.000 -0.012 0.027
^4D	32211.9 32235.1 32808.7 34255.6 34725.4	0.003 -0.001 -0.034 -0.454 -0.486	-0.002 0.001 0.034 0.454 -0.486
^2I	33961.9 34112.7 35727.2 35734.6 36499.6 36597.6 36868.7 37175.3 37363.4 37745.6 39588.4 39899.4 39906.2	0.000 0.000 0.000 0.000 0.000 0.000 0.000 0.000 0.000 0.000 0.000 0.000 0.000	0.000 0.000 0.000 0.000 0.000 0.000 0.000 0.000 0.000 0.000 0.000 0.000 0.000

Figure S12 NEVPT2 transition spectrum of the complexes **1 - 3**.

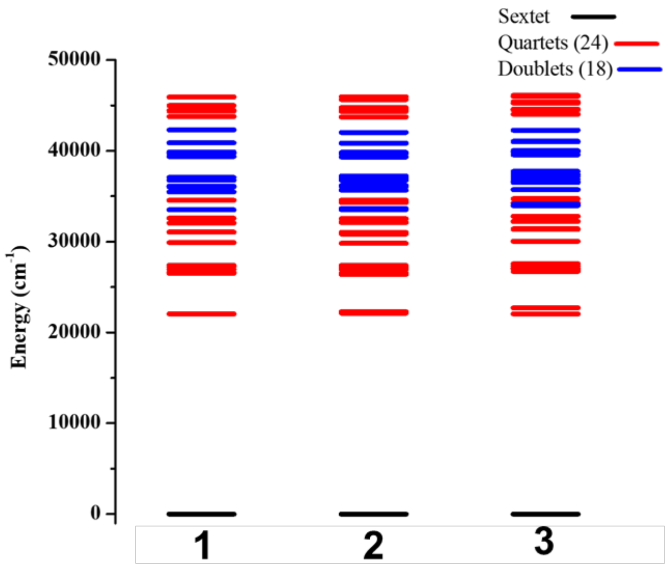

Figure S13 Diagrammatic representation of the representation of the five d-orbitals of complex **1**.

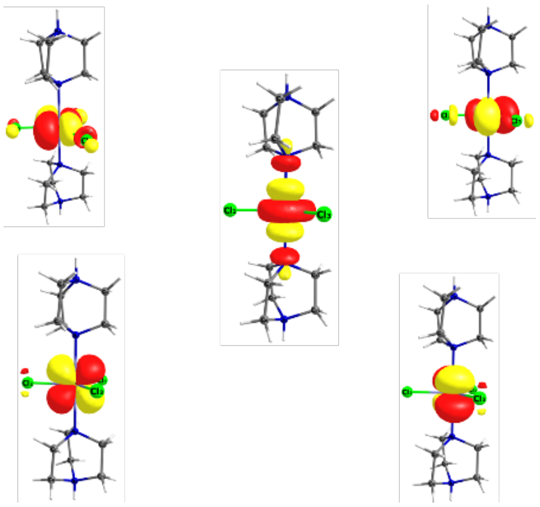

Table S8 Combination of *ab initio* spin-orbit coupling (SOC) and DFT computed spin-spin (SS) results for the D parameter. The DFT computed SOC values are provided purely for comparison *(see discussion in main text).*

Complex	$D^{\text{NEVPT2-SOC}}$ (cm^{-1})	$D^{\text{SS-BP86}}$ (cm^{-1})	$D^{\text{SOC-BP86}}$ (cm^{-1})*	D^{net} (cm^{-1})
1	–0.112	–0.021	–0.308*	–0.133
2	–0.113	–0.024	–0.312*	–0.137
3	–0.108	–0.021	-0.295*	–0.129

*The $D^{\text{SOC-BP86}}$ values have not been included in the D^{net} value as they are significantly overestimated. Therefore $D^{\text{net}} = D^{\text{SOC-NEVPT2}} + D^{\text{SS-BP86}}$ *(see discussion in main text).*

Table S9 Bond length parameters, NEVPT2 transition energies and ZFS parameters of the model complex.

Model Complexes	**Avg. Mn-N bond length (Å)**	**Energy of the 1st & 2nd excited quartet (cm^{-1})**	**Contribution to *D* value from the 1st & 2nd excited quartet (cm^{-1})**	**D_{SOC} (cm^{-1})**	***E*/*D***
Complex **2** (original)	2.38	22141 & 22286	–0.314 & –0.303	–0.113	0.036
2.1	2.30	20761 & 20936	–0.357 & –0.345	–0.149	0.034
2.2	2.25	19773 & 19950	–0.387 & –0.374	–0.184	0.033
2.3	2.20	18677 & 18856	–0.420 & –0.406	–0.228	0.032
2.4	2.15	17470 & 17644	–0.457 & –0.442	–0.284	0.030
2.5	2.10	16158 & 16330	–0.501 & –0.484	–0.353	0.030
2.6	2.05	14742 & 14911	–0.552 & –0.534	–0.440	0.030
2.7	2.00	13232 & 13396	–0.616 & –0.595	–0.558	0.030
2.8	1.90	9971 & 10115	–0.805 & –0.775	–0.917	0.029
2.9	1.80	6492 & 6599	–1.189 & –1.140	–1.687	0.028

Figure S14 Magneto structural correlation of Mn-N bond length with first two excited quartet energy levels computed from NEVPT2.

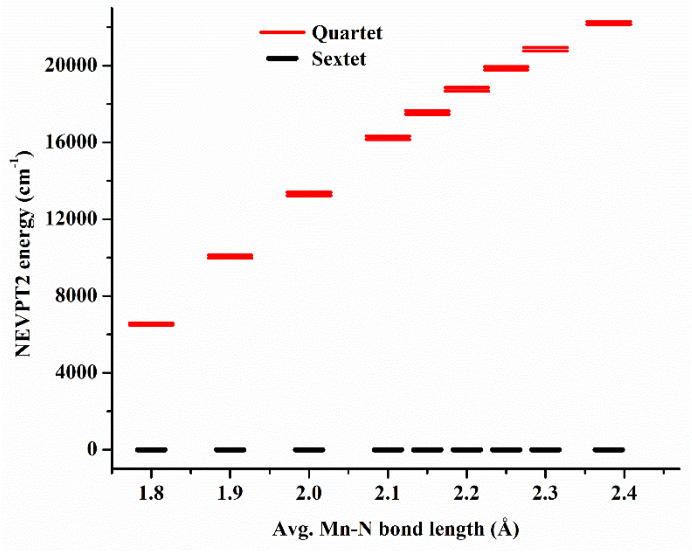

References

(1) M. Pinsky and D. Avnir, *Inorg. Chem.* **1998**, *37*, 5575–5582.

(2) D. Casanova, J. Cirera, M. Llunell, P. Alemany, D. Avnir and S. Alvarez, *J. Am. Chem. Soc.* **2004**, *126*, 1755–1763.

(3) N. F. Chilton, R. P. Anderson, L. D. Turner, A. Soncini and K. S. Murray, *J. Comput. Chem.* **2013**, *34*, 1164–1175.

(4) F. Neese, *Wiley Interdiscip. Rev. Comput. Mol. Sci.* **2018**, *8*, e1327.

(5) F. Neese, *Wiley Interdiscip. Rev. Comput. Mol. Sci.* **2011**, *2*, 73–78.

(6) R. Maurice, R. Bastardis, C. de Graaf, N. Suaud, T. Mallah, and N. Guihéry, *J. Chem. Theory Comput.* **2009**, *5*, 2977–2984.